Dynamic Analysis of a Novel Zero-Stiffness Vibration Isolator by Considering Frictional Force Involved

Kan Ye[1(✉)], J. C. Ji[1], and Ding Hu[2]

[1] School of Mechanical and Mechatronic Engineering, University of Technology Sydney, 15 Broadway, Ultimo, NSW, Australia
kan.ye@uts.edu.au

[2] Shanghai Institute of Applied Mathematics and Mechanics, Shanghai University, 266 Jufengyuan Rd, Baoshan, Shanghai, China

Abstract. This study proposes a novel zero-stiffness vibration isolator and investigates its dynamic responses under micro-oscillation with a friction consideration. The novel vibration isolator is based on the mechanism of a cam-roller Quasi-Zero-Stiffness (QZS) system while with improvement by reducing its system components. The proposed vibration isolator consists of a designed bearing, which can provide stiffness responses in the radial direction, and an inserted rod with curved surface. Without the precise cooperation between the positive and negative stiffness systems required in a typical QZS isolator, the designed single stiffness system can provide the high-static-low-dynamic stiffness characteristic directly. The static characteristics of the stiffness performance are numerically confirmed, and then the dynamic responses with friction consideration at the contact surfaces are discussed. The displacement transmissibility in low frequency range is numerically validated when applying harmonic excitation on the base. The analysis results of this study reveal a unique vibration isolating performance of the zero-stiffness system under frication consideration.

Keywords: Zero-stiffness · Vibration isolator · Friction consideration · Displacement transmissibility

1 Introduction

Nonlinear QZS vibration isolation systems have been proposed to overcome the disadvantage of a traditional linear isolator [1, 2]. A typical QZS system is combined by a linear isolation system and a negative stiffness structure, thus a high-static-low-dynamic stiffness (HSLDS) can be generated for the effective vibration isolation in a low frequency range. Different types of the stiffness system such as springs [3, 4], buckled beams [5] and magnetic springs [6], have been used individually, or in various combinations for both positive and negative stiffness structures. The dynamic response of the QZS isolation systems have been extensively studied for isolating low-frequency vibrations, in which the lamped mass model and Harmonic Balance Method are used

X. Jing et al. (Eds.): ICANDVC 2021, LNEE 799, pp. 544–553, 2022.
https://doi.org/10.1007/978-981-16-5912-6_40

frequently for analysis [4, 7]. Other models, such as the finite element model, are also used based on the structure type [8].

This study proposes a novel zero-stiffness vibration isolator that can achieve the high-static-low-dynamic stiffness characteristic directly without precise cooperation between the positive and negative stiffness systems. The proposed vibration isolator is based on the cam-roller mechanism [9, 10] and consists of a designed bearing, which can provide stiffness responses in the radial direction, and an inserted rod with special curved surface, as shown in Fig. 1(a) and (b). The design concept of the bearing and the static characteristics of the isolator are first presented, and then nonlinear dynamic performance with a friction consideration [11, 12] at the connect surface is evaluated.

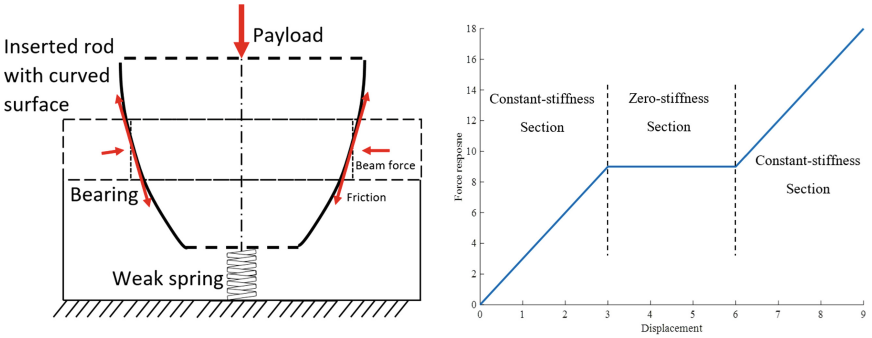

Fig. 1. Schematic diagram of the system: (a) system configuration and (b) force-displacement relationship.

2 The Model of the Zero-Stiffness System

There are two systems involves in this novel design for a zero-stiffness performance: a bearing design and a curved rod as shown in Fig. 1(a). The bearing structure is designed based on cantilevered beams, which are limited deformable in the horizontal plane. One end of the beam is fixed on the outer ring of the structure and a hemisphere roller is placed on the other end. When the curved rod is inserted, the contact of the rod surface and the hemisphere balls could perform a cam-roller mechanical principle. Thus, the stiffness in the vertical direction can be designed according to the rod surface curve and a HSLDS characteristic can be achieved when using for vibration isolation. The benefits of proposed system are: firstly, the system size can be reduced when comparing to other spring structures. Higher stiffness can be obtained when using the cantilevered beam structure with less deformation. Secondly, the system stiffness can be designed sectional as Demands. Even a zero-stiffness performance can be resulted as shown in Fig. 1(b) when special rod shape is achieved. It should be noting that a weak spring ($k \approx 0$) is also applied to define the initial position of the rod in zero-stiffness section for vibration application. The following sections of this paper will demonstrate the designing the system and its static performance, and then the dynamic performance will be discussed.

2.1 Designing of the Structure and Static Performance

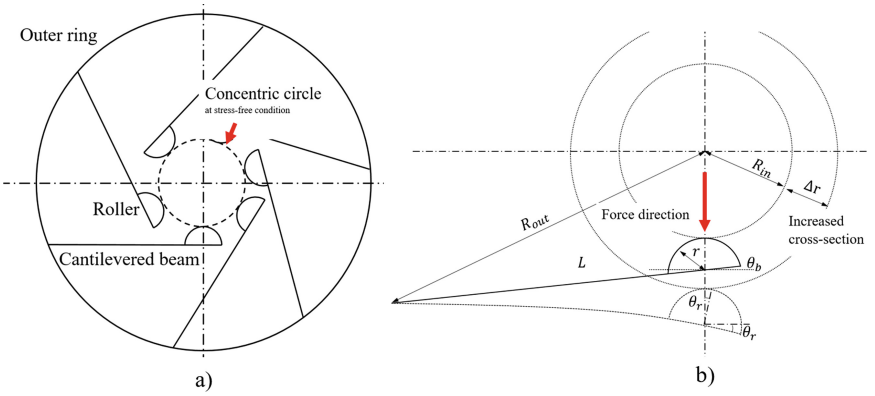

Fig. 2. Mechanism of the proposed bearing structure: (a) top view and (b) deformed condition.

As presented in Fig. 2, the designed bearing could include N sets of cantilevered beam-roller. When inserting a rod at the center of the outer ring, the contact points of each hemisphere roller to the cross-section of the inserted rod should be on a concentric circle with the outer ring. Considering geometrically-trigonometric relationships of the rollers and the neglecting the small deformation of the cantilevered beams, the maximum number of the beam-roller set can have the relationship as:

$$\frac{\pi}{N_{max}} \geq \sin^{-1}\left(\frac{r}{\mathrm{R}_{in}+r}\right) \tag{1}$$

where R_{in} is initial radius of the concentric circle when the beams are at stress-free condition, and r is the radius of the hemisphere roller.

To minimize the size of the bearing and the system, the relation between maximum number of the beam-roller set and the ratio of R_{in} and r can be calculated as shown in Fig. 3. It can be found that the higher ratio of R_{in}/r could using more beam-roller set in the bearing system which could bring more radiation stiffness of the bearing k_h and provide higher equivalent negative stiffness in the vertical direction.

It also can be found that the minimum size of the radius of the outer ring structure, R_{out}, can be the relationship as:

$$\mathrm{R}_{out}{}^2 = (L\cos(\theta_b))^2 + (L\sin(\theta_b) + \mathrm{R}_{in} + r)^2 \tag{2}$$

where as shown in the Fig. 2(b), L is the effective length of the cantilevered beam, which is calculated from the support location to the center of the roller and θ_b is the angle between the beam surface and the possible force direction from the rod to the roller.

When rod is inserted with its cross-section larger than the initial radius of the concentric circle, $\mathrm{R}_{in} + \Delta r$, the cantilevered beam can be forced at the roller center with a

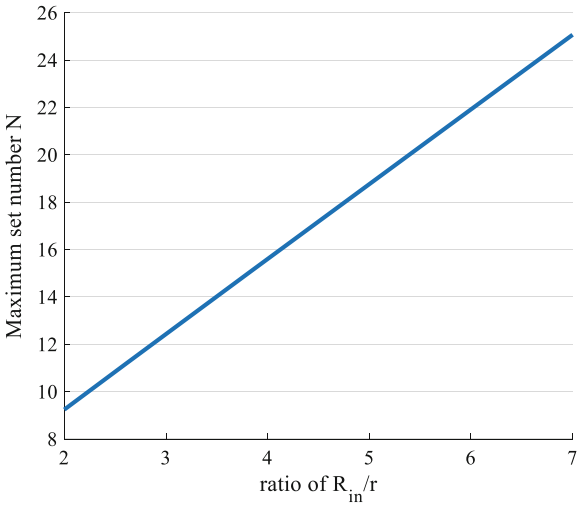

Fig. 3. Maximum number of the beam-roller set with in the system.

deformation. Thus, the equivalent total radiation stiffness of the bearing k_h due to the deformation of the cantilevered beams can be calculated as

$$k_h = N\frac{Ebh^3}{4L^3 cos(\theta_b)} \tag{3}$$

where a rectangle cross-section beam is assumed to be applied, b and h are the width and thickness of the beam, and E is the elastic module of the beam material.

It is also worth noting that the direction of the force applied on the beam has an angle change due to the roller contact,θ_r as shown in the Fig. 2(b). Only when θ_r is small and can be neglected, the force applied to the beam can be assumed in the vertical direction. Otherwise, when θ_r is big, the force applied perpendicular to the beam surface is calculated as

$$P = F\cos(\theta_b - \theta_r) and \theta_r = \frac{PL^2}{2EI} \tag{4}$$

where $I = \frac{1}{12}bh^3$ is the moment of inertia of the beam, F is the force applied on the roller, and P is the force applies perpendicular to the beam.

By substituting the Eq. (4) into Eq. (1), a required radiation stiffness k_h, the outer radius of the bearing can be rewritten as

$$R_{out} = \sqrt{\left(\sqrt[3]{N\frac{Ebh^3}{4k_h cos(\theta_b)}}cos(\theta_b)\right)^2 + \left(\sqrt[3]{N\frac{Ebh^3}{4k_h cos(\theta_b)}}sin(\theta_b) + R_{in} + r\right)^2} \tag{5}$$

where N must satisfy the minimum requirement as shown in the Eq. (1).

Figure 4 illustrates the Inclined angle analysis of the beams within the bearing structure for required stiffness K_h. This analysis is based on using spring steel beams.

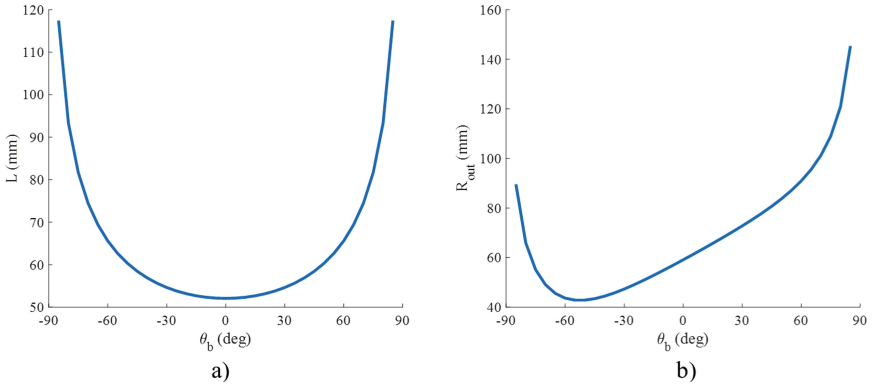

Fig. 4. Inclined angle analysis of the beams within the bearing structure for required stiffness to minimize the bearing size.

Particular design parameters are given as: $E = 205GPa, b = 8\,mm, h = 3\,mm, r = 4\,mm$, $R_{in} = 24\,mm$, $N = 20$ and $K_h = 160\,N/m$. It is clearly shown that although the minimum length of the beam can be required when $\theta_b = 0$, its outer ring size is not at its minimum. For the given design parameters, the minimum size of the outer ring can be achieved when $\theta_b = -50$.

2.2 Designing of the Curved Rod

The inclined angle of the touching surface on the shaped rod could decide the transformation ratio of the total raboth the natural frequency diation stiffness to the resultant stiffness in vertical direction (Fig. 5).

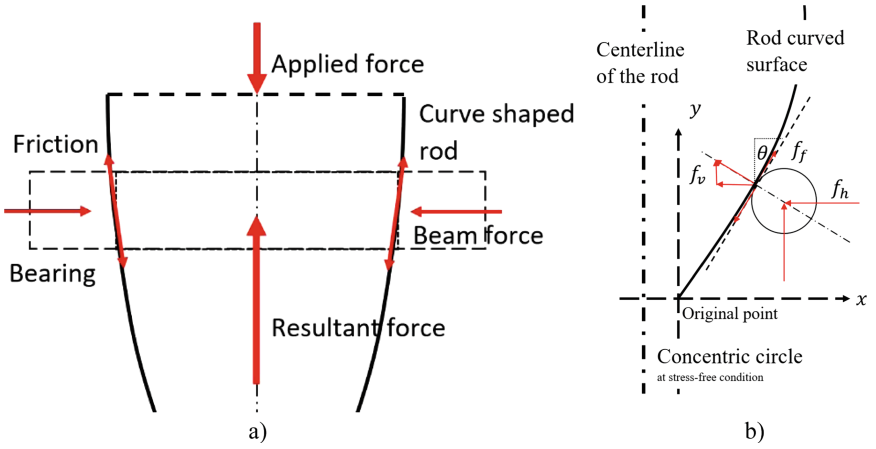

Fig. 5. (a) Mechanism of the bearing-rod system and (b) the rod inclined curve.

If the rod surface curve is expressed as:

$$y(x) = A(x)^B \tag{6}$$

The equivalent vertical stiffness k_v can be rewritten as:

$$k_v = k_h \left(\frac{\left(\left(\frac{y}{A}\right)^{\frac{1}{B}}\right)^{1-B} \left\{ 2\left(\frac{y}{A}\right)^{\frac{1}{B}} + \delta - B\left[\left(\frac{y}{A}\right)^{\frac{1}{B}} + \delta\right]\right\}}{AB^2 y} \right) \tag{7}$$

where A and B are algebraic constants, δ is the pre-compression condition of the beam at the original point of the curve.

It is worth noting that special curve conditions could result different equivalent vertical stiffness as demand: when B = 1, the rod would be presented as a cone shaped rod, and the equivalent vertical stiffness can be simplified to a constant $k_v = \frac{k_h}{A^2}$; when $B = 2 \& \delta = 0$, a zero-stiffness condition $k_v = 0$ can be achieved along the rod. The combination of the two special curve conditions thus can provide the desired stiffness in the vertical direction along the rod, the stiffness static performance of proposed system then could be able as shown in Fig. 1(b). it is ideally that the vibration can be totally isolated to the load platform at the zero-stiffness section. However, for any real engineer application, the frictions involved in the cam-roller system should not be neglected as it can directly effect on the dynamic response.

3 Dynamic Analysis with Friction Consideration

The designed zero-stiffness system would be investigated with a Coulomb friction consideration at its contact surface between the rod and the roller. Although the proposed system is a single-degree-of-freedom system, its dynamic behavior still can be complicated as nonlinearities due to the friction consideration and the unsymmetrical curved shape.

According to the geometry relationship at the contact surface, the equation of motion along the rod can be expressed as:

$$m\ddot{z_m} + ky + \mu mg\left(2\sqrt{C_R y}\right) sgn\left(\dot{U}\right) = 0 \tag{8}$$

where k is the vertical stiffness of the system and it equal to 0 while within the zero-stiffness section, μ is the frictional coefficient, g is the gravity constant, C_R is the curve constant (same as A in Eq. (6)), y is the location of the contact point along the rod from the original point, $\dot{U}$ denotes the absolute speed of the roller to the rod, and $\ddot{z_m}$ denote the absolute acceleration of the weight.

Suppose that a steady-state can be reached for the proposed system in a frictional oscillator. The displacement of the payload can be exhibited to the same period of the excitation. A time interval $\left[0\ 2\pi/\omega_b\right]$ can be found between a generic couples of subsequent maximum value, which could represent the steady-state of the motion. An

unknown phase shift is also expected between the excitation and the response. Assuming that the motion is continuous and symmetric with respect to the initial position of the contact between the rod and the rollers, the absolute speed of the roller to the rod at all internal points within the half time interval $\left[0\ \pi/\omega_b\right]$ from the maximum displacement to the minimum condition are always negative $\dot{U} < 0$, so Eq. (8) will be rewritten as:

$$\ddot{U} - C_1\sqrt{1+U} = C_2\cos(\omega_b t + \varphi) \tag{9}$$

where $C_1 = 2\mu g\left(\frac{\sqrt{C_R}}{\sqrt{y_0}}\right)$, $C_2 = \frac{Z_e{\omega_b}^2}{y_0}$ and ω_b is the excitation frequency. It also should be noted that the initial position y_0, which is defined by the weak spring and the phase angle φ of the excitation are both unknown.

An analytical solution using Taylor series expansion with keeping up to the third-order about its initial position can be succinctly written as:

$$\ddot{U} - C_1\left(1 + \frac{U}{2}\right) = C_2\cos(\omega_b t + \varphi) \tag{10}$$

The end boundary conditions of both displacement and velocity in a half time period $\left[0\ \pi/\omega_b\right]$ can be found as:

$$\begin{cases} U_{(0)} = U_0 \quad \dot{U}_{(0)} = 0 \\ U_{\left(\frac{\pi}{\omega_b}\right)} = -U_0\ \dot{U}_{\left(\frac{\pi}{\omega_b}\right)} = 0 \end{cases} \tag{11}$$

As solving the general solution of Eq. (10), the response regarding to the time interval can be expressed as:

$$U_{(t)} = \left(-\frac{2}{C_1}{\omega_n}^2\right)[A_n\cos(\omega_n t) + B_n\sin(\omega_n t)] - 2\left[1 + \frac{C_2}{C_1}\cos(\omega_b t + \varphi)\right] \tag{12}$$

where ω_n is the natural frequency of the system for a target weight m. Since the system would provide a zero-stiffness, the calculation of its natural frequency is depending on the initial position of the contact of the rod and the roller, where $\omega_n = \sqrt{g/y_0}$.

The constants A_n and B_n can be then removed by bring $U_{(t)}$ into its boundary conditions $U_{(0)}$ and $\dot{U}_{(0)}$, So

$$U_{(t)} = \left(U_0 + 2\frac{C_2}{C_1}\cos(\varphi) + 2\right)\cos(\omega_n t) - 2\frac{C_2}{C_1}\frac{\omega_b}{\omega_n}\sin(\varphi)\sin(\omega_n t) - 2\left[1 + \frac{C_2}{C_1}\cos(\omega_b t + \varphi)\right] \tag{13}$$

Substituting the response result into the impositions of the boundary condition at time interval $\frac{\pi}{\omega_b}$ allows to finding the unknown values of the phase angle φ, hence:

$$\begin{cases} \cos(\varphi) = -\frac{1}{2}\frac{C_1}{C_2}U_0 \\ \sin(\varphi) = -\frac{C_1}{C_2}\frac{1}{\alpha}\frac{\sin(\frac{\pi}{\alpha})}{\cos(\frac{\pi}{\alpha})+1} \end{cases} \tag{14}$$

where $\alpha = \omega_b/\omega_n$.

By introducing a damping function $D_{(\alpha)} = \frac{1}{\alpha}\frac{\sin(\frac{\pi}{\alpha})}{\cos(\frac{\pi}{\alpha})+1}$, the maximum absolute displacement U_0 can be determined as

$$U_0 = 2\sqrt{\left(\frac{C_2}{C_1}\right)^2 - D_{(\alpha)}{}^2} \tag{15}$$

It should be noted that as for continuous motion, $\dot{U}_{(t)} < 0$ at $t \in \left[0\ \frac{\pi}{\omega_b}\right]$; substituting the $\cos(\varphi)$ and $\sin(\varphi)$, a unique limit condition for the validity of the maximum absolute displacement U_0 can be obtained, which is independently of the ratio between friction and external force:

$$U_0 > \frac{-2\omega_n sin(\omega_n t) + 2D\omega_b[cos(\omega_n t) - cos(\omega_b t)]}{\omega_b sin(\omega_b t)} \tag{16}$$

It must be underlined that the friction response has been considered over the response of the weak spring applied for initial position, and which has been neglected when analysis the dynamic behavior within the zero-stiffness section. The numerical solution of the amplitude-frequency relationship can be calculated and shown in Fig. 6 to investigate the system dynamic response. However, the response under the limit condition as shown

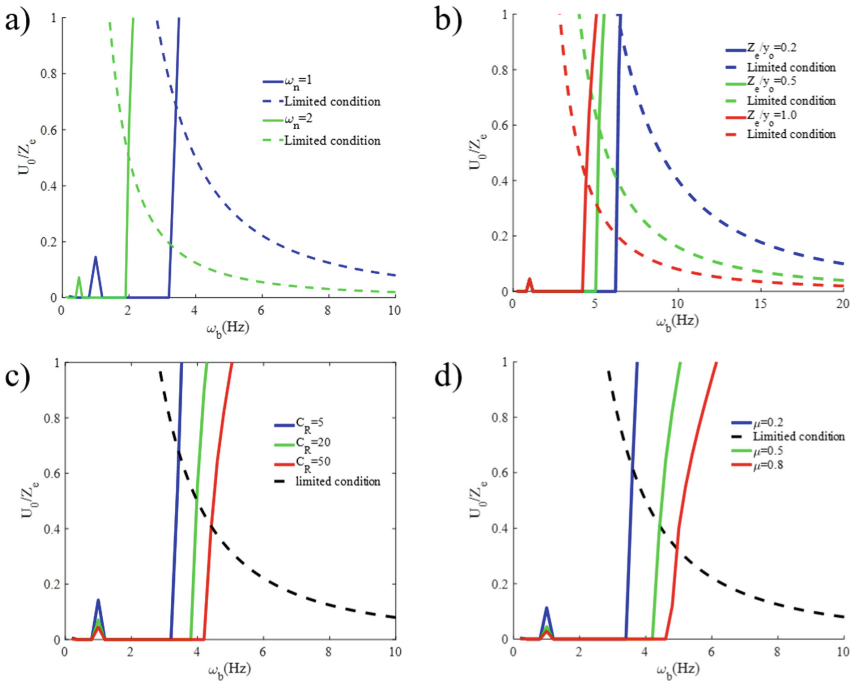

Fig. 6. Displacement transmissibility of the proposed system with frictional consideration with different designing parameters: (a) natural frequency of the system ω_n; (b) excitation amplitude Z_e; (c) rod curve constant C_R and (d) frictional coefficient μ

in Eq. (16) cannot be captured in the analytic solution. Only the displacement transmissibility with respect to the excitation frequency within the limit condition are discussed. From Fig. 8, the effects of the designing parameters, such as natural frequency of the system ω_n, rod curve constant C_R, frictional coefficient μ and the excitation amplitude Z_e to the AF response can be found, respectively.

According to Fig. 6 (a–b), both the natural frequency of the system ω_n, which is depending on the initial position of the contact of the rod and the roller, and the excitation amplitude Z_e can be found to decide the unique limit condition in the nonlinear dynamic analysis. Either low natural frequency or large excitation amplitude could increase the range within the limited condition, and in the meantime reduce the workable isolation frequency range. Other parameters which can have significant effect on the vibration isolation performance are also simulated and presented in Fig. 6(c)–(d). The increasing of either the frictional coefficient μ or the rod curve constant C_R are able to increase the workable isolation range of the system.

4 Conclusions

A HSLDS vibration isolation system is proposed with a novel designed bearing and a curved surface rod. The designed system omits the precise cooperation between the positive and negative stiffness systems in a typical QZS system and is able to provide a high-static-low-dynamic stiffness directly. The design concept and its static characteristics of the stiffness performance have been numerically confirmed and discussed. A zero-stiffness-in-range property at the targeted weight applied can be achieved ideally. Then nonlinear dynamic performance under micro-oscillation with a friction consideration is also evaluated. The analysis results of this study reveal a unique vibration isolating performance of the zero-stiffness system under frication consideration.

References

1. Ding H, Ji J, Chen L-Q (2019) Nonlinear vibration isolation for fluid-conveying pipes using quasi-zero stiffness characteristics. Mech Syst Signal Process 121:675–688
2. Ye K, Ji J, Brown T (2020) Design of a quasi-zero stiffness isolation system for supporting different loads. J Sound Vib 471:115198
3. Zhao F, Ji J, Ye K, Luo Q (2020) Increase of quasi-zero stiffness region using two pairs of oblique springs. Mech Syst Signal Process 144:106975
4. Lu Z, Brennan M, Ding H, Chen L (2018) High-static-low-dynamic-stiffness vibration isolation enhanced by damping nonlinearity. SCIENCE CHINA Technol Sci 62(7):1103–1110. https://doi.org/10.1007/s11431-017-9281-9
5. Huang X, Liu X, Sun J, Zhang Z, Hua H (2014) Vibration isolation characteristics of a nonlinear isolator using Euler buckled beam as negative stiffness corrector: a theoretical and experimental study. J Sound Vib 333:1132–1148
6. Yan B, Ma H, Zhao C, Wu C, Wang K, Wang P (2018) A vari-stiffness nonlinear isolator with magnetic effects: theoretical modeling and experimental verification. Int J Mech Sci 148:745–755
7. Zheng J, Yang X, Xu J, Zhou W, Lu Y, Liu L (2020) A novel of low-frequency vibration isolation with high-static low-dynamic stiffness characteristic. Iranian J Sci Technol Trans Mech Eng 45(3):597–609. https://doi.org/10.1007/s40997-020-00370-9

8. Yao H, Wang Y, Xie L, Wen B (2020) Bi-stable buckled beam nonlinear energy sink applied to rotor system. Mech Syst Signal Process 138:106546. https://doi.org/10.1016/j.ymssp.2019.106546
9. Zhou J, Wang X, Xu D, Bishop S (2015) Nonlinear dynamic characteristics of a quasi-zero stiffness vibration isolator with cam–roller–spring mechanisms. J Sound Vib 346:53–69
10. Xu D, Yu Q, Zhou J, Bishop S (2013) Theoretical and experimental analyses of a nonlinear magnetic vibration isolator with quasi-zero-stiffness characteristic. J Sound Vib 332:3377–3389
11. Liu X, Zhao Q, Zhang Z, Zhou X (2019) An experiment investigation on the effect of Coulomb friction on the displacement transmissibility of a quasi-zero stiffness isolator. J Mech Sci Technol 33(1):121–127. https://doi.org/10.1007/s12206-018-1212-7
12. Marino L, Cicirello A, Hills DA (2019) Displacement transmissibility of a Coulomb friction oscillator subject to joined base-wall motion. Nonlinear Dyn 98(4):2595–2612. https://doi.org/10.1007/s11071-019-04983-x